A Robust Low-Cost EEG Motor Imagery-Based Brain-Computer Interface

Shivanthan A.C. Yohanandan, Isabell Kiral-Kornek, Jianbin Tang, Benjamin S. Mashford, Umar Asif, and Stefan Harrer (*IEEE Senior Member*), *IBM Research, Melbourne, Australia*

Abstract—Motor imagery (MI) based Brain-Computer Interfaces (BCIs) are a viable option for giving locked-in syndrome patients independence and communicability. BCIs comprising expensive medical-grade EEG systems evaluated in carefully-controlled, artificial environments are impractical for take-home use. Previous studies evaluated low-cost systems; however, performance was suboptimal or inconclusive. Here we evaluated a low-cost EEG system, OpenBCI, in a natural environment and leveraged neurofeedback, deep learning, and wider temporal windows to improve performance. μ-rhythm data collected over the sensorimotor cortex from healthy participants performing relaxation and right-handed MI tasks were used to train a multi-layer perceptron binary classifier using deep learning. We showed that our method outperforms previous OpenBCI MI-based BCIs, thereby extending the BCI capabilities of this low-cost device.

Keywords—brain-computer interface; motor-imagery; locked-in syndrome; deep learning; neurofeedback

I. INTRODUCTION

Locked-in syndrome (LIS) patients can consciously perceive the world around them despite their inability to move or communicate due to a near-complete paralysis of muscles [1]. Brain-Computer Interfaces (BCIs) have been proposed as a method to facilitate interaction with the world, using brain activity alone to control external devices [2]–[5]. Due to its non-invasiveness, scalp electroencephalography (EEG) is a commonly used method to measure neural activity [6]. EEG-based BCIs comprise three primary modalities: steady-state visually evoked potentials, the P300 waveform, and motor imagery (MI). MI is most suitable and practical for LIS patients since the other modalities require functional muscular activity [7].

Despite previous efforts, high-performing BCIs are confined to carefully-controlled, noise-free, artificial environments, and are heavily dependent on expensive medical-grade systems [8]. These conditions are impractical for typical BCI target users, who spend most of their time in noisy, interference-prone natural environments. Consequently, studies evaluated MI using the OpenBCI system: a low-cost portable BCI. However, reported accuracies were close to chance (Agarwal *et al.* [9] reported 53.4% mean accuracy), environmental conditions were unclear (Agarwal *et al.* [9], Belwafi *et al.* [10], and Suryotrisongko *et al.* [11] did not describe their experimental environment), or sample sizes were small or biased (Belfawi *et al.* (80% mean accuracy) used a sample size of four participants, including two with prior MI training).

Neurofeedback training, absent from these studies, has been proposed to improve BCI performance by providing users with real-time self-regulated neural activity feedback [7]. Therefore, neurofeedback has the potential to improve the quality of MI data. Furthermore, deep learning, a machine learning technique using multi-layered artificial neural networks to learn rules from structured data, has had notable success in MI classification [12]–[15]. Finally, temporal window size, defined as the duration a user is required to imagine movement, has been shown to correlate positively with accuracy and thus further improve performance [16], [17].

To that end, this study evaluated MI classification using OpenBCI and employed neurofeedback, deep learning, and long imagery duration to improve performance over similar studies. The remainder of this paper is structured as follows: Section II describes our methods, covering the experimental data collection (II A), neurofeedback (II B), pre-processing strategies (II C), and description of a deep learning classifier (II D). Section III presents the results that are subsequently discussed in Section IV, and Section V concludes the study.

II. METHODS

A. Data Acquisition

Seven human volunteers participated in the experiment and gave their informed consent. Experimental procedures were designed and carried out in accordance with the Declaration of Helsinki and approved by the Institutional Review Board.
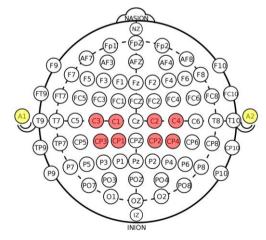

Figure 1: International 10/10 electrode configuration used to maximize μ-rhythm detection. Red represents 8 EEG voltage recording electrodes and yellow represents reference (A1) and common-mode noise rejection bias/ground (A2) electrodes.

Eight passive gold cup electrodes (OpenBCI) coated with conductive paste (Weaver Ten20) were secured to the scalp using a neoprene cap as per the international 10/10 EEG configuration shown in Fig. 1. This configuration covers the sensorimotor region, which is recommended for high-quality μ-rhythm detection [7]. Raw EEG data from 8 channels were wirelessly (low-energy Bluetooth) acquired by a laptop PC at 250 Hz using the OpenBCI Cyton Biosensing 32-bit board and custom-built software written in Python.

The visual cue-based experimental paradigm consisted of two MI tasks: baseline mental relaxation and imagined right-handed movement. Tasks lasted 10 seconds and were interleaved in an alternating manner over a single 10-minute session, guided by the software interface (Fig. 2). Consequently, EEG data labelling was synchronized with visual cues from the software. To balance the dataset, an equal number of relaxation and right-handed imagery movements was considered. The experiment was conducted in a standard office meeting room to mimic a natural indoor environment and participants were seated comfortably on a chair facing a laptop screen.
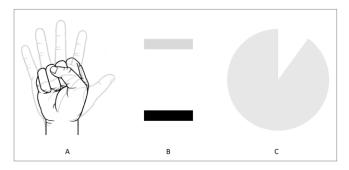

Figure 2: Custom-built data acquisition and neurofeedback training software interface (written in Python). A visual cue to relax (gray open-hand) or imagine right-handed movement (black closed-hand) is toggled in region A. A rising (mental relaxation) or falling (right-handed imagery) horizontal bar (B) provided real-time MI feedback. A 10-second countdown timer is displayed in region C.

B. Neurofeedback

The change in amplitude of μ-rhythms during self-regulated voluntary movements has gained considerable interest as a potential electrophysiological signal for EEG-based BCIs [18]. These variations of synchronization of cortical rhythms are referred to as event-related desynchronization (ERDs) and synchronization (ERSs) [19]. When imagining hand movement, the μ-band exhibits a decrease in amplitude, or ERD. Conversely, when the imagined movement ceases, the brain exhibits an increase in μ-band amplitude [20], [21], or ERS. Leveraging this phenomenon, we developed software capable of displaying ERDs and ERSs back to the user in real-time.

Visual feedback of self-regulated MI neural activity was provided to participants by way of a floating horizontal bar (Fig. 2B) updated every second. Bar height was computed by calculating the μ-rhythm frequency band (7–13 Hz) spectral power averaged across all 8 electrode channels (Equation 1).

$$\mu_{power} = \frac{1}{8} \sum_{i=1}^{8} \int_{7\,\text{Hz}}^{13\,\text{Hz}} X_i(f)\, df \qquad (1)$$

Where i is the electrode channel, $X_i(f) = \mathcal{F}\{(x_i)\}$, and $\mathcal{F}$ is the discrete Fourier transform of the raw channel time-series signal x_i.

Participants were instructed to move the bar downwards (Fig. 2B black bar) by imagining a prolonged right-handed movement, or upwards (Fig. 2B gray bar) by relaxing during the 10-second task duration. Previous studies instructed participants to imagine a fixed routine (e.g., hand-squeeze action), which has proven to be unreliable [9]–[11]. Here, we leveraged neurofeedback training to allow users to experiment with different imagery strategies (e.g. hand *movement*) to identify the most successful one in real-time.

C. Data Pre-Processing

A third-order zero-phase Butterworth bandpass filter was applied between 0.1–100 Hz and notch-filtered at 50 Hz to suppress line noise across all 8 electrode channels. Sample values exceeding $\pm 6\sigma$, where σ is the standard deviation of any given voltage trace, were set to $\pm 6\sigma$ to rectify outliers in voltage. This pre-processing method has previously been described in detail by Kiral-Kornek *et al.* [2]. The labelled 10-minute time-series voltage data from all 8 electrode channels from each participant were split into chronological 10-second blocks. These blocks were further split into W-subsets comprising samples of equal window size (in seconds), W, where $W \in \{1,2,3,4,5,6,7,8,9\}$.

To maximize dataset size for training a deep learning classifier, a sliding window of size W and a stride of 4 *ms* (one sample) was used to generate more samples within each 10-second block. Time-series data were then transformed into the frequency domain by performing an FFT on each W-length sample to compute μ-rhythm band-limited spectral power, resulting in 15,060–135,060 8-dimensional vector training samples within each W-subset.

D. Deep Learning Classification

A multi-layer fully-connected perceptron network scoring high (98.2% accuracy) on the MNIST hand-written digit classification task was implemented on CPU/GPU platforms using the deep learning framework TensorFlow [22] to classify relaxation and right-handed imagery. This classifier was chosen because the 8-dimensional training samples resembled low-level hand-written digit features. Data epochs from each W-subset were randomly shuffled and split into training (75% of samples) and test (25% of samples) sets, and fed into the network (one for each participant) in batches of 100. Weights were learned using slow gradient decent over 100 epochs. The base learning rate was set to 0.05, and decreased by a factor of 10 after 2000 iterations, with the final layer trained with 25% dropout. Network performance was evaluated by computing the classification accuracy (correct classifications / total classifications) of the trained model on the held-out test set for each W-length subset. Network topology and hyperparameters are summarized in Table 1.

Hyperparameter	Value
Hidden units in first layer	200
Hidden units in second layer	100
Hidden units in third layer	60
Hidden units in fourth layer	30
Units in fifth (output) layer	2
Batch size	100
Training epochs	100
Base learning rate	0.05
Max learning rate	0.5
Dropout	25%

Table 1: Multi-layer perceptron network topology and hyperparameters.

III. RESULTS

Fig. 3 shows the temporal evolution of μ-rhythm power computed from a single electrode channel (CP3) from a single participant (P006) over 30 seconds. Event-related synchronizations during mental relaxation increased μ-band amplitude, resulting in increased μ-power (first and last 10 seconds). Conversely, imagined motor activity decreased μ-band power (middle 10 seconds) resulting from event-related desynchronization.
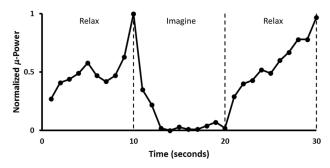

Figure 3: μ-rhythm spectral power temporal evolution computed for a single electrode channel (CP3) from a single participant (P006) over 30 seconds of alternating relax-imagine-relax time-series data.
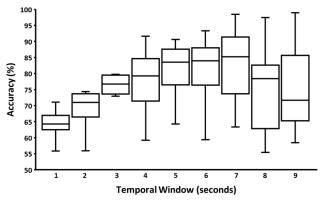

Figure 4: Boxplot showing classification accuracies across 7 participants as a function of temporal window size. Horizontal lines represent medians, top and bottom whiskers represent maximum and minimum, respectively, and boxed regions represent 25th to 75th percentile data.

Classification accuracies as a function of temporal window size, W, are tabulated in Table 2 for each participant, and represented more concisely in Fig. 4. At the group level, median accuracy increased with imagery duration up to 7 seconds, before decreasing approaching 9 seconds. The minimum and maximum accuracy across the 7 participants was 55.46% (1 second temporal window) and 98.96% (9 seconds temporal window), respectively. A two-tailed paired Student's t-test revealed no statistically significant improvement beyond 5 seconds duration. Hence, this point appears to mark the optimal tradeoff between imagery duration and accuracy (~83%).

IV. DISCUSSION

In this work, we evaluated methods for neurofeedback training, varying imagery duration, and deep learning for classifying relaxation vs. imagined motor-related EEG data using the OpenBCI system. We found that neurofeedback training seemed to improved classification accuracy. This was expected since participants could identify successful motor-imagery strategies during data collection and labelling, consequently generating high-quality training samples for classification.

We also found that classification accuracy increased with temporal window size up to 7 seconds. Fig. 3 affords us a possible explanation for this behavior. When users begun the imagination task by self-regulating neural activity, their corresponding μ-rhythm response was gradual and had a cumulative effect over the duration of the task. When the task was switched, the same effect was observed, albeit in the opposite direction. Therefore, longer imagery durations captured prolonged μ-rhythm activity, yielding higher classification accuracies. This was expected since imagery duration may increase classification confidence and thus accuracy. Accuracy was found to decrease beyond 7 seconds, possibly due to a decrease in the number of training examples. The possibility to vary the window duration provides users with a mechanism to prioritize either speed or accuracy.

Compared to previous studies that investigated MI classification using the OpenBCI system [9]–[11], we emphasized the experimental environment by taking into account the impact of environmental parameters (e.g. audible noise, distractions, and electromagnetic interference) and therefore demonstrated the robustness of our system in interference-prone environments. We also demonstrated that our system achieved higher classification accuracy than Agarwal et al. [9] and Suryotrisongko et al. [11] by increasing temporal window size. Belfawi et al. [10] reported a group mean accuracy of 80%; nevertheless, their relatively small sample size (n = 4) does not allow direct comparison. It is important to note that although we achieved superior classification accuracy, this came at a latency cost. However, we believe this further improves the robustness of BCIs, which is essential for practical use in real-life situations.

		Temporal Window (seconds)								
		1	2	3	4	5	6	7	8	9
Participant	001	*55.46*	55.96	59.72	59.17	64.27	59.37	63.37	62.82	63.58
	002	63.02	64.56	72.91	71.52	70.70	85.32	91.29	55.85	97.21
	003	65.24	68.26	74.31	71.30	82.28	70.33	66.79	62.83	66.95
	004	64.25	73.10	79.28	84.87	89.13	90.74	91.51	84.01	58.48
	006	71.08	85.20	93.03	91.64	90.62	93.36	98.49	97.48	***98.96***
	007	68.71	74.35	79.80	84.47	86.11	83.94	80.58	78.42	71.71
	008	62.01	70.99	76.74	79.29	83.52	82.37	85.24	81.27	74.05
		64.25	**71.09**	**76.74**	**79.30**	**83.53**	**83.94**	**85.25**	**78.43**	**71.71**

Table 2: Classification accuracies (%) across all 7 participants as a function of temporal window size (imagery duration). Medians shown in boldface (bottom row) and minimum and maximum shown in italicized boldface.

V. Conclusion

In this paper, we demonstrated the successful implementation of a covert binary movement classifier for classifying EEG using the OpenBCI system. We found classification accuracy increases with imagery duration, and leveraged deep learning and neurofeedback to outperform previous similar studies. This system constitutes a low-cost and robust motor imagery-based classification system for EEG signals, enabling accessible brain-computer interfacing for individuals with locked-in syndrome in their natural environment. Future work involves validating this system in a low-power processing environment as could be provided by IBM's TrueNorth neurosynaptic chip system [23].

Acknowledgment

References

[1] J. R. Patterson and M. Grabois, "Locked-in syndrome: a review of 139 cases.," *Stroke*, vol. 17, no. 4, pp. 758–764, Jul. 1986.

[2] I. Kiral-Kornek *et al.*, "TrueNorth-enabled real-time classification of EEG data for brain-computer interfacing," in *2017 39th Annual International Conference of the IEEE Engineering in Medicine and Biology Society (EMBC)*, 2017, pp. 1648–1651.

[3] E. Nurse, B. S. Mashford, A. J. Yepes, I. Kiral-Kornek, S. Harrer, and D. R. Freestone, "Decoding EEG and LFP Signals Using Deep Learning: Heading TrueNorth," in *Proceedings of the ACM International Conference on Computing Frontiers*, New York, NY, USA, 2016, pp. 259–266.

[4] J. R. Wolpaw and D. J. McFarland, "Control of a two-dimensional movement signal by a noninvasive brain-computer interface in humans," *Proc. Natl. Acad. Sci. U. S. A.*, vol. 101, no. 51, pp. 17849–17854, Dec. 2004.

[5] U. Chaudhary, B. Xia, S. Silvoni, L. G. Cohen, and N. Birbaumer, "Brain–Computer Interface–Based Communication in the Completely Locked-In State," *PLOS Biol.*, vol. 15, no. 1, p. e1002593, Jan. 2017.

[6] S. Waldert, "Invasive vs. Non-Invasive Neuronal Signals for Brain-Machine Interfaces: Will One Prevail?," *Front. Neurosci.*, vol. 10, Jun. 2016.

[7] L. F. Nicolas-Alonso and J. Gomez-Gil, "Brain Computer Interfaces, a Review," *Sensors*, vol. 12, no. 2, pp. 1211–1279, Jan. 2012.

[8] C. M. McCrimmon *et al.*, "A small, portable, battery-powered brain-computer interface system for motor rehabilitation," in *2016 38th Annual International Conference of the IEEE Engineering in Medicine and Biology Society (EMBC)*, 2016, pp. 2776–2779.

[9] M. Agarwal and R. Sivakumar, "THINK: Toward Practical General-Purpose Brain-Computer Communication," in *Proceedings of the 2Nd International Workshop on Hot Topics in Wireless*, New York, NY, USA, 2015, pp. 41–45.

[10] K. Belwafi, R. Djemal, F. Ghaffari, O. Romain, B. Ouni, and S. Gannouni, "Online Adaptive Filters to Classify Left and Right Hand Motor Imagery," in *Proceedings of the International Joint Conference on Biomedical Engineering Systems and Technologies*, Portugal, 2016, pp. 335–339.

[11] H. Suryotrisongko and F. Samopa, "Evaluating OpenBCI Spiderclaw V1 Headwear's Electrodes Placements for Brain-Computer Interface (BCI) Motor Imagery Application," *Procedia Comput. Sci.*, vol. 72, pp. 398–405, Jan. 2015.

[12] X. An, D. Kuang, X. Guo, Y. Zhao, and L. He, "A Deep Learning Method for Classification of EEG Data Based on Motor Imagery," in *Intelligent Computing in Bioinformatics*, 2014, pp. 203–210.

[13] N. Lu, T. Li, X. Ren, and H. Miao, "A Deep Learning Scheme for Motor Imagery Classification based on Restricted Boltzmann Machines," *IEEE Trans. Neural Syst. Rehabil. Eng.*, vol. 25, no. 6, pp. 566–576, Jun. 2017.

[14] J. Li and A. Cichocki, "Deep Learning of Multifractal Attributes from Motor Imagery Induced EEG," in *Neural Information Processing*, 2014, pp. 503–510.

[15] Y. R. Tabar and U. Halici, "A novel deep learning approach for classification of EEG motor imagery signals," *J. Neural Eng.*, vol. 14, no. 1, p. 016003, 2017.

[16] R. A. Block, "Remembered duration: Imagery processes and contextual encoding," *Acta Psychol. (Amst.)*, vol. 62, no. 2, pp. 103–122, Jun. 1986.

[17] N. Naseer and K. S. Hong, "Determination of temporal window size for classifying the mean value of fNIRS signals from motor imagery," in *2013 6th IEEE Conference on Robotics, Automation and Mechatronics (RAM)*, 2013, pp. 237–240.

[18] Y. Jeon, C. S. Nam, Y.-J. Kim, and M. C. Whang, "Event-related (De)synchronization (ERD/ERS) during motor imagery tasks: Implications for brain–computer interfaces," *Int. J. Ind. Ergon.*, vol. 41, no. 5, pp. 428–436, Sep. 2011.

[19] C. Neuper and G. Pfurtscheller, "Evidence for distinct beta resonance frequencies in human EEG related to specific sensorimotor cortical areas," *Clin. Neurophysiol.*, vol. 112, no. 11, pp. 2084–2097, Nov. 2001.

[20] G. Pfurtscheller, W. Sager, and W. Wege, "Correlations between CT scan and sensorimotor EEG rhythms in patients with cerebrovascular disorders," *Electroencephalogr. Clin. Neurophysiol.*, vol. 52, no. 5, pp. 473–485, Nov. 1981.

[21] W. Gaetz and D. Cheyne, "Localization of sensorimotor cortical rhythms induced by tactile stimulation using spatially filtered MEG," *NeuroImage*, vol. 30, no. 3, pp. 899–908, Apr. 2006.

[22] M. Abadi *et al.*, "TensorFlow: A system for large-scale machine learning," 2016.

[23] F. Akopyan *et al.*, "TrueNorth: Design and Tool Flow of a 65 mW 1 Million Neuron Programmable Neurosynaptic Chip," *IEEE Trans. Comput.-Aided Des. Integr. Circuits Syst.*, vol. 34, no. 10, pp. 1537–1557, Oct. 2015.